Effects of boundary columns on the seismic behavior of cantilever structural walls

S. Kono
Materials and Structures Laboratory, Tokyo Institute of Technology, Japan

K. Sakamoto, M. Sakashita
Dept. of Architecture and Architectural Engineering, Kyoto University, Japan

T. Mukai, M. Tani and H. Fukuyama
Building Research Institute, Japan

SUMMARY:
In order to study effects of boundary columns and their confinement on the seismic performance of structural walls, four 40%-scale cantilever type structural walls with or without boundary columns were tested with two levels of end-region shear reinforcement. The total area of barbel-shape and rectangular sections, the area of confined area, and the moment capacity were set equal and designed to fail in flexure mode. The test results showed that it was efficient to provide boundary columns to reduce damage level and increase the ultimate drift capacity. It was also made clear that the axial force level needs to be reduced and the section end should be well confined when a structural wall with rectangular section is designed.

Keywords: Cantilever RC structural walls, boundary columns, confinement, ultimate deformation

1. GENERAL INSTRUCTIONS

In the 2010 Chile Off Maule Earthquake, a number of structural walls failed in flexure in major cities like Santiago, Vina Del Mar, Concepcion, and etc. It was observed that concrete crushing spread at more than half of the wall width and vertical reinforcement buckled or fractured near compression or tension fibre. Before the earthquake, it was considered that cantilever type structural walls would behave much better although some researchers reported characteristic failure modes of structural walls experimentally observed at the ultimate condition. The observed damage patterns at post-earthquake investigations was so brittle and extensive that structural engineers had to reconsider a false belief that structural walls always behave well.

Japanese structural walls normally have boundary columns and beams to provide good confinement to wall panels. In addition to the confining effect, boundary columns carry a large amount of axial force to reduce axial stress level of wall panels to reduce their damage.

In order to study effects of boundary columns on the seismic performance of structural walls, four 40%-scale cantilever type structural walls with or without boundary columns were tested with two levels of the end-region shear reinforcement. The total area of wall section, the area of confined end zone, the moment capacity were made equal for all specimens. The moment capacities of structural walls were set at least 1.5 times higher than the shear capacities so that all specimens fail in flexure. In this manner, static loading test was conducted to study the effect of boundary columns and confining shear reinforcement on the hysteresis characteristics, such as post-peak backbone curve, ductility, and failure mode. The test results showed that it was efficient to provide boundary columns to reduce damage level. It was also made clear that the axial force level needs to be reduced and the section end be well confined when a structural wall is designed without boundary columns.

2. EXPERIMENTAL WORK

2.1. Test setup

Four 40% scale specimens are prepared by changing the configuration of section (barbell-shape and rectangular sections) and amount of shear reinforcement as shown in **Figure 1**. Specimens BC40 and BC80 had boundary columns and NC40 and NC80 had no boundary columns. Four specimens had same width (1,750mm), and nearly same section area (2,250cm^2 for BC's and 2,240cm^2 for NC's) and confined end zone (625cm^2 for BC's and 666cm^2 for NC's). Based on the Japanese design guidelines (AIJ 1999), their ultimate drift angle, ${}_cR_u$, varies from 1.00 to 2.40 as listed in **Table 1**. The table also lists major test variables. The shear capacity is set more than 1.5 time larger than the flexural capacity for all specimens so that they fail in flexure mode. The computed maximum flexural capacities are listed as ${}_cQ_{max}$ in **Table 4**. Longitudinal reinforcement at confined region was anchored to an 18mm thick plate. The wall panel was divided into four regions (Z1, Z2, Z3 and Z4) in the vertical direction so that shear and flexural deformations were measured separately. **Table 2** and **Table 3** list the mechanical properties of concrete and reinforcement. Loading system is shown in **Figure 2**. The lateral load was applied at the center of the top loading beam, which is 3000 mm high from the top of the foundation. Hence, the shear span ratio was 1.71. The axial force of 1500 kN was applied constantly by two hydraulic jacks to keep the axial load level of 0.20 for confined region, that is, 0.11 for the total area of the section.

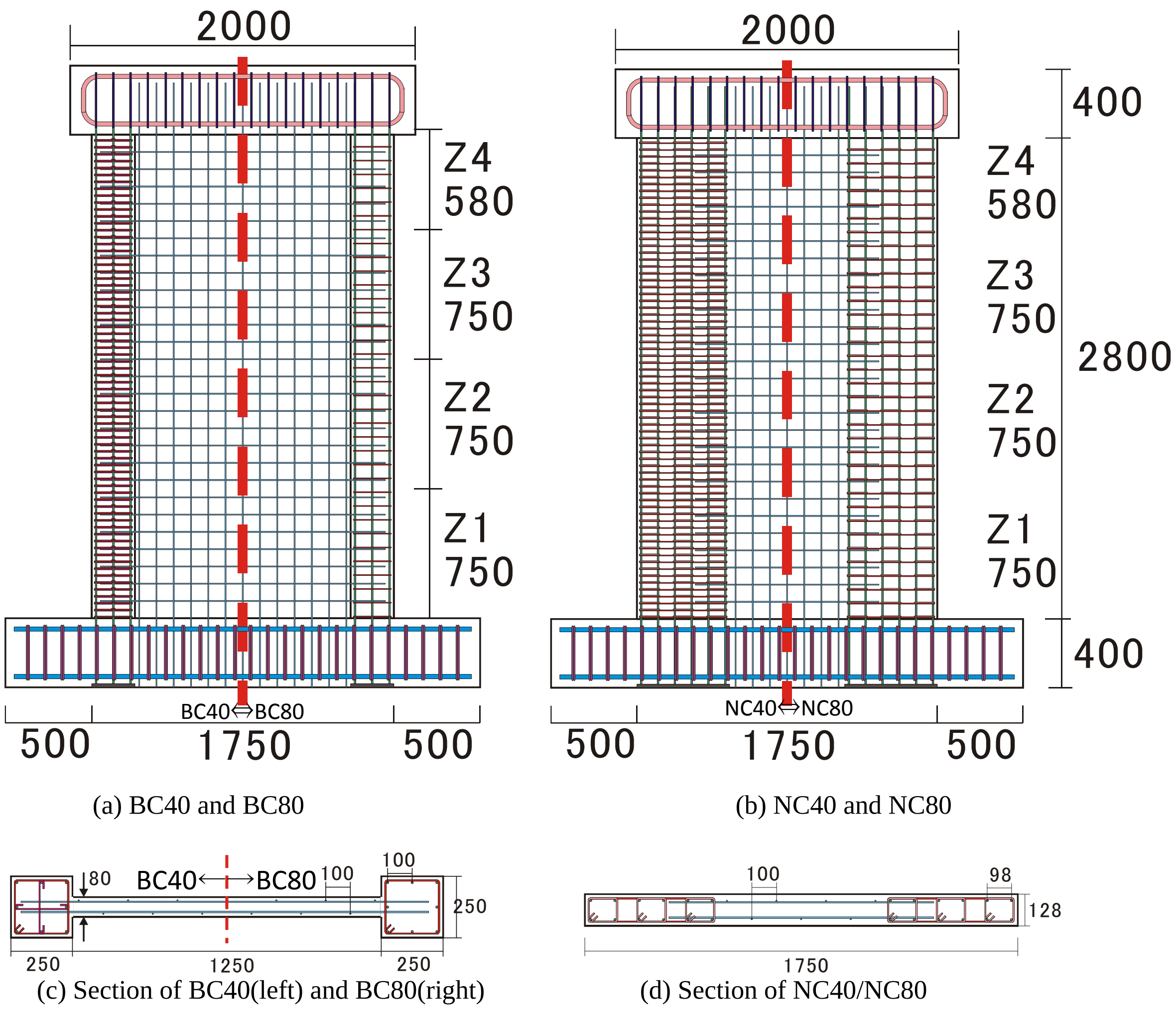

Figure 1. Dimensions and reinforcement of specimens (Unit: mm)

Table 1. Variables of specimens

Specimen	Width & height (mm)	Confined area			Wall panel		$_cR_u$ (%)
		Section dimension (mm)	Longitudinal reinforcement (rebar ratio)	Shear reinforcement (rebar ratio)	Thickness (mm)	Shear reinforcement (rebar ratio)	
BC40	1750 2800	250x250	8-D10 (0.91%)	3-D6@40 (0.95%)	80	D6@100 Staggered (0.40%)	2.40
BC80				2-D6@80 (0.32%)			1.29
NC40		128x520	12-D10 (1.29%)	3.2-D6@40 (1.98%)	128	D6@100 Staggered (0.25%)	1.72
NC80				3.2-D6@80 (0.99%)			1.00

'$_cR_u$' denotes the flexural component of the ultimate drift angle based on AIJ guidelines (AIJ, 1999).

Table 2. Mechanical properties of concrete

Specimen	Compressive strength (MPa)	Young's modulus (GPa)	Splitting strength (MPa)
BC40, BC80	59.5	30.9	5.10
NC40, NC80	52.5	30.1	3.66

Table 3. Mechanical properties of reinforcement

Reinforcement	Yield strength (MPa)	Young's modulus (GPa)	Tensile strength (MPa)
D6	387	189	496
D10	377	194	533

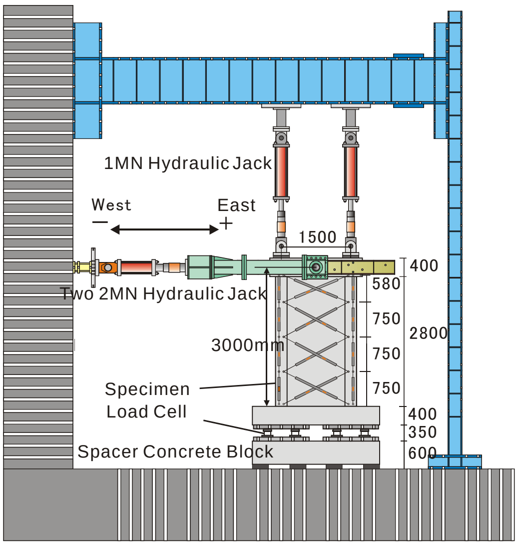

(a) Dimensions and setup (Unit: mm)

(b) Photo of the loading system

Figure 2. Loading system

2.2. Test results

Figure 3 shows lateral load - drift angle relations. All specimens yielded in flexure, reached the peak point, and deformed until the failure without too much degradation of lateral load carrying capacity. The ultimate failure was caused by the crushing of confined concrete. It is interesting that all hysteresis curves had very small residual drift at most cycles. Small residual drift is probably due to high concrete strength and axial force which made specimens behave like post-tensioned precast concrete structures. The detail discussion on this issue will be made elsewhere. The figures show the characteristic points (cracking, yielding, peak load, and ultimate deformation) by different marks. The ultimate deformation is defined by either 20% degradation of load carrying capacity from the peak or the maximum drift. Values of these characteristic points are listed in **Table 4**. BC40 and BC80 show no degradation of load carrying capacity until the failure but NC40 and NC80 show some degradation due to crushing of core concrete.

Figure 4 shows the contribution from flexure and shear deformations to the drift. Drift due to flexural or shear deformation of four regions (Regions Z1 to Z4 in **Figure 1**) is expressed in percentage. Z0 is the lower 50mm region which has vertical displacement gages to measure pullout of vertical reinforcement. Z1' is the virtual zone where flexural deformation of Z0 was subtracted from Z1. The flexural contribution was constantly as high as 80% for NC40 and NC80 while it changes from 50 - 60 % for small drift angle to 80% for larger drift angles for BC40 and BC80. It is noted that contribution of shear deformation is large before yielding when the boundary columns are provided. On the other hand, contribution of shear deformation is not very large when the wall had no boundary columns since the flexural deformation is dominant.

Table 4. Comparison between experimental results and computed values.

Specimen		Flexural cracking				Yielding of long. Rebar				Maximum capacity				Ultimate drift			
		$_eQ_{cr}$ (kN) (1)	$_eR_{cr}$ (%) (2)	$_cQ_{cr}$ (kN) (3)	η_{cr} (1)/(3)	$_eQ_y$ (kN) (4)	$_eR_y$ (%) (5)	$_cQ_y$ (kN) (6)	η_y (4)/(6)	$_eQ_{max}$ (kN) (7)	$_eR_{max}$ (%) (8)	$_cQ_{max}$ (kN) (9)	η_{max} (7)/(9)	$_eR_u$ (%) (10)	$_eR_{uf}$ (%) (11)	$_cR_{uf}$ (%) (12)	η_{uf} (11)/(12)
BC40	+	+443	+0.12	288	1.54	+562	+0.29	479	1.17	+634	+1.41	568	1.12	+4.00	+2.99	3.21	0.93
	−	-441	-0.10		1.53	-521	-0.25		1.09	-608	-1.47		1.07	(-2.75)	(-1.70)		—
BC80	+	+418	+0.08	290	1.44	+487	+0.26	482	1.01	+633	+1.17	563	1.12	+2.00	+1.31	1.59	0.82
	−	-338	-0.07		1.17	-507	-0.33		1.05	-592	-1.45		1.05	(-2.00)	(-1.37)		—
NC40	+	+328	+0.07	200	1.64	+478	+0.19	431	1.11	+606	+1.91	567	1.07	+2.38	+1.75	1.53	1.14
	−	-379	-0.09		1.90	-449	-0.20		1.04	-604	-1.46		1.07	(-2.00)	(-1.59)		—
NC80	+	+334	+0.09	201	1.66	+467	+0.30	434	1.08	+598	+1.16	558	1.07	+1.50	+1.16	1.06	1.09
	−	-331	-0.08		1.65	-332	-0.12		0.76	-578	-0.87		1.04	(-1.50)	(-1.12)		—

Left subscripts '*e*' and '*c*' denote experimental and computed values, respectively. Capital letters *Q* and *R* denote load and drift angle, respectively. $_eR_u$ is the experimental total drift angle , $_eR_{uf}$ the experimental flexural drift angle and $_cR_{uf}$ is computed flexural drift angle based on Sec. 2.2.

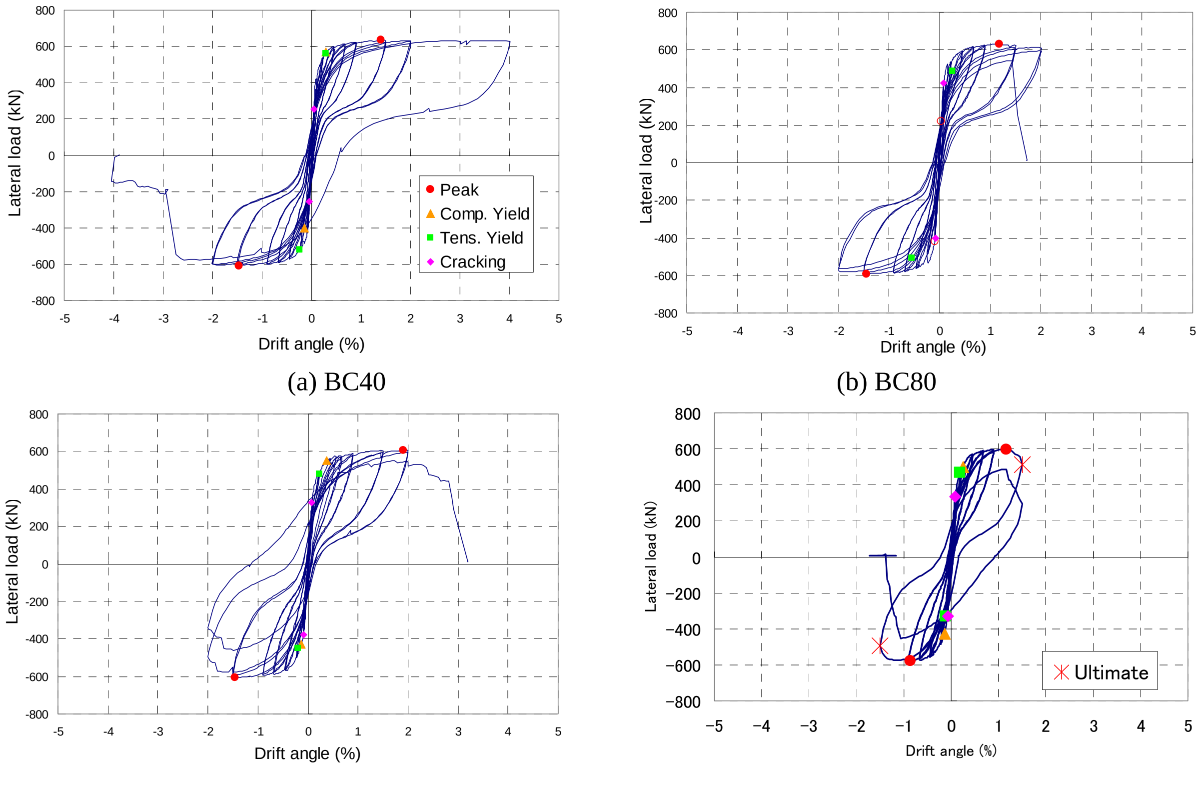

(a) BC40 (b) BC80

(c) NC40 (d) NC80

Figure 3. Lateral load - drift angle relation

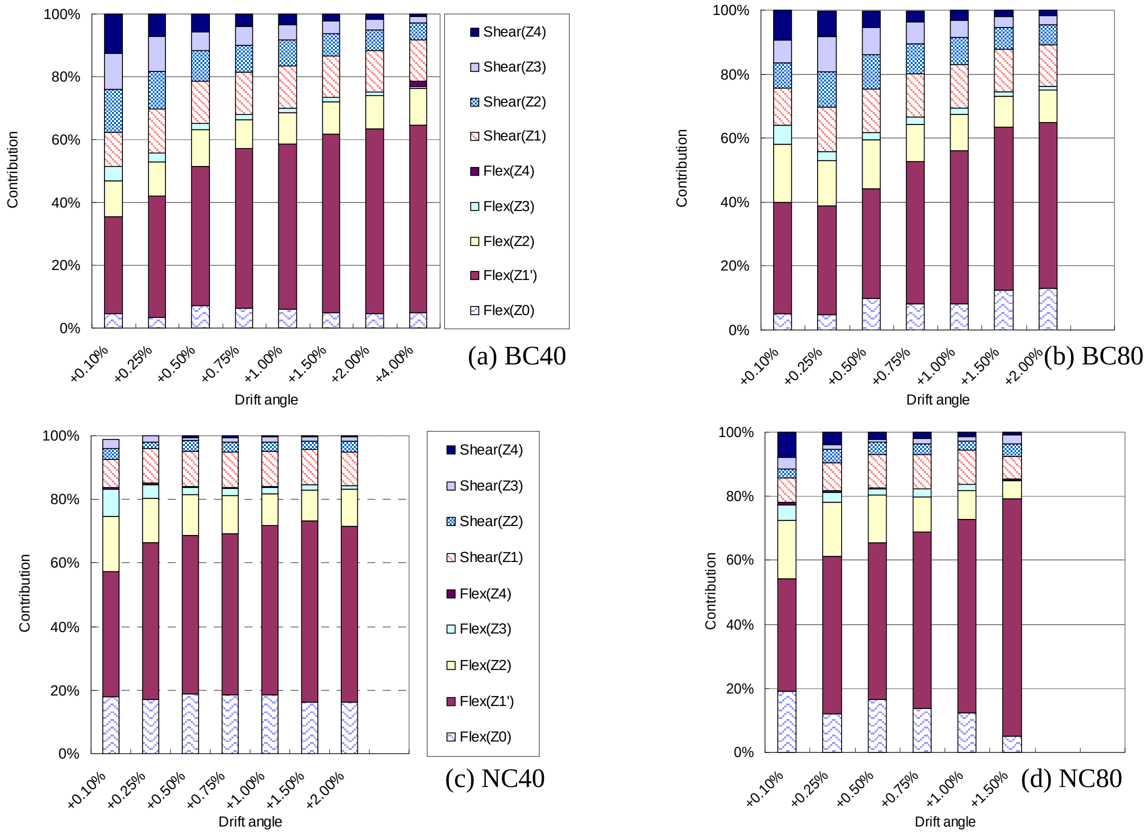

Figure 4. Contribution from flexure and shear deformations to the drift

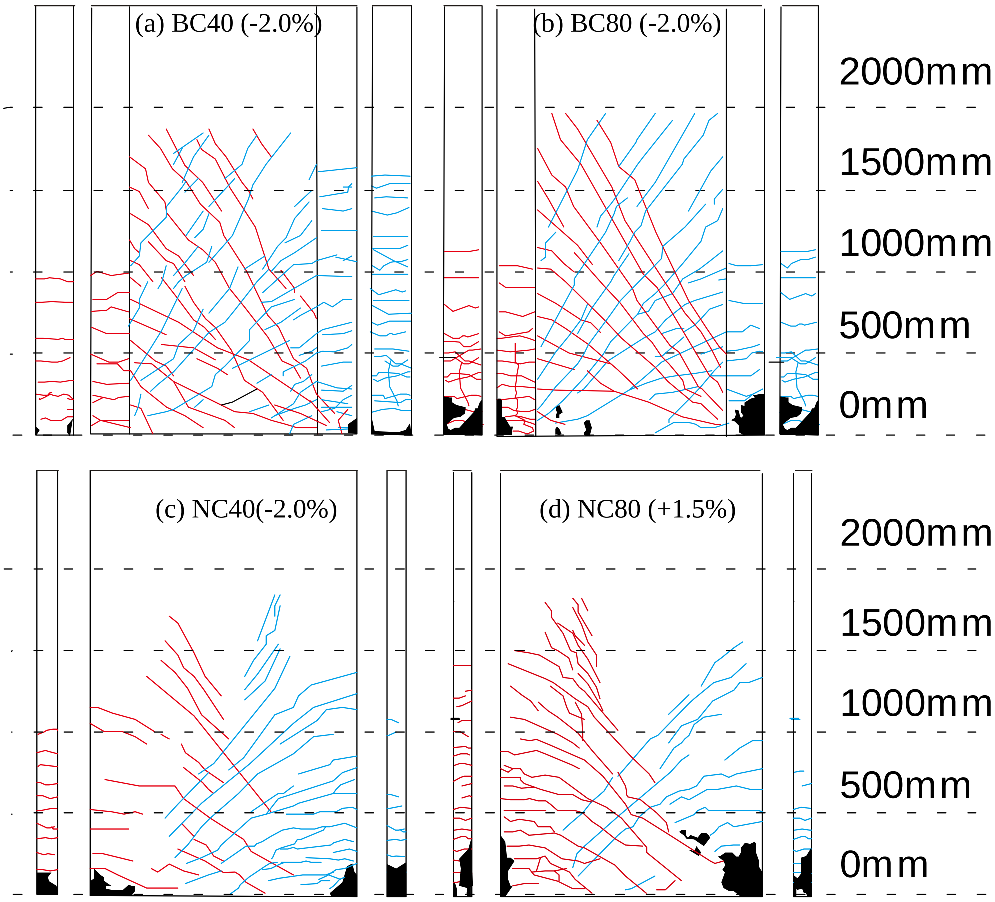

Figure 5. Crack patterns at peak load

Figure 5 shows crack patterns at the final cycle. Red and blue lines represent cracks in positive and negative directions, respectively. NC40 and NC80 have flexure-shear cracks which are basically continuous. Although BC40 and BC80 have flexure-shear cracks, flexural cracks and shear cracks are not necessarily continuous at the column interface. At the final stage, the failure was brittle since core concrete crushed in a brittle manner. Crushing happed only at the boundary column for BC40 and BC80. However, crushing of concrete extended to the center of the wall panel for NC40 and NC80 and wall panels buckled at the compression region as was seen for the 2010 Chile EQ. Buckling of longitudinal reinforcement at compression region was observed for all specimens.

3. ANALYTICAL WORK

Lateral load - drift angel (flexural component) is computed using fiber analysis (Sec. 2.1) and the ultimate drift angle was obtained based on the limit compressive strain (Sec. 2.2).

3.1. Derivation of the lateral load - drift angle (flexural component) relations

A typical fiber model was used in the analysis. The wall section was divided into 175 concrete elements in width direction. Each longitudinal reinforcement was modelled as an independent steel element. Concrete elements have stress-strain relations as shown in **Figure 6**(a). Plain concrete has Popovics' model (Popovics 1973) for a rising branch and linear line for a falling branch where the strain at zero stress was taken as 0.005. Confined concrete is expressed by Sakino and Sun's model (Sakino and Sun 1994).

Flexural component of drift angle, R_f, was computed by **Eq. (1)** based on the curvature distribution in **Figure 6**(b). The curvature is divided into elastic and plastic curvatures. Each curvature was used to derive elastic drift, δ_e, and plastic drift, δ_p, as **Eqs. (2)** and **(3)**.

$$R_f\,(\%) = \frac{\delta_e + \delta_p}{H} \times 100 \qquad \textbf{(1)}$$

$$\delta_e = \frac{Q \cdot H^3}{3EI} \qquad \textbf{(2)}$$

$$\delta_p = \frac{1}{2}\phi_p (l_p)^2 + \phi_p (l_p)(H - l_p) \qquad \textbf{(3)}$$

where Q is the lateral load, H the wall height (3000 mm), E Young's modulus of concrete, I the second moment of inertia of the wall section, ϕ_p the plastic curvature, l_p the plastic hinge length. After the parametric study, l_p was fixed to 350mm, which is 0.2 times wall width (1750mm). The plastic hinge length corresponds to the yielding of longitudinal reinforcement and curvature distribution observed in the experiment.

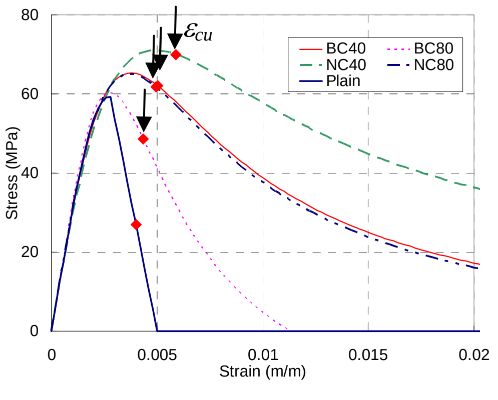

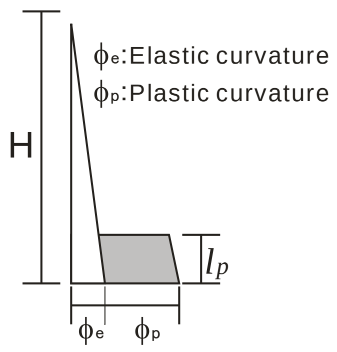

(a) Stress - strain relations (b) Curvature distribution along vertical axis

Figure 6. Stress - strain relations for plain and confined concrete and idealized curvature distribution

The ultimate drift was computed based on the limit compressive strain, ε_{cu}, proposed by Mander et al (Mander et al. 1988).

$$\varepsilon_{cu} = 0.004 + \frac{1.4\rho_s f_{yh}\varepsilon_{sm}}{f'_{cc}} \tag{4}$$

where ρ_s is the volumetric ratio of confining reinforcement to core concrete, f_{yh} the yield strength of confining reinforcement, ε_{sm} the fracture strain of confining reinforcement and 0.005 was used, f'_{cc} the compressive strength of confined concrete. In the analysis, when the centroid of the column (125 mm from the compressive fibre) reached the limit compressive strain, ε_{cu}, the analysis was terminated and the corresponding drift was considered to be the ultimate drift for BC40 and BC80. For NC40 and NC80, the element 125 mm from the compressive fibre was also checked. This corresponds to the centroid of equivalent square which has same section area with confined rectangular area.

3.2. Comparison between computed backbone curves to experimental results

The computed relation between lateral load, Q, and flexural component of drift angle, R_f, is compared with the experimental hysteresis curve in **Figure 7**. The characteristic points such as cracking, yielding, peak, and ultimate are compared in **Table 4**. Although the computed peak load is smaller than the experimental value, the computed backbone curve well simulates the envelop of the experimental results. It is noted that the ultimate drift is especially well simulated.

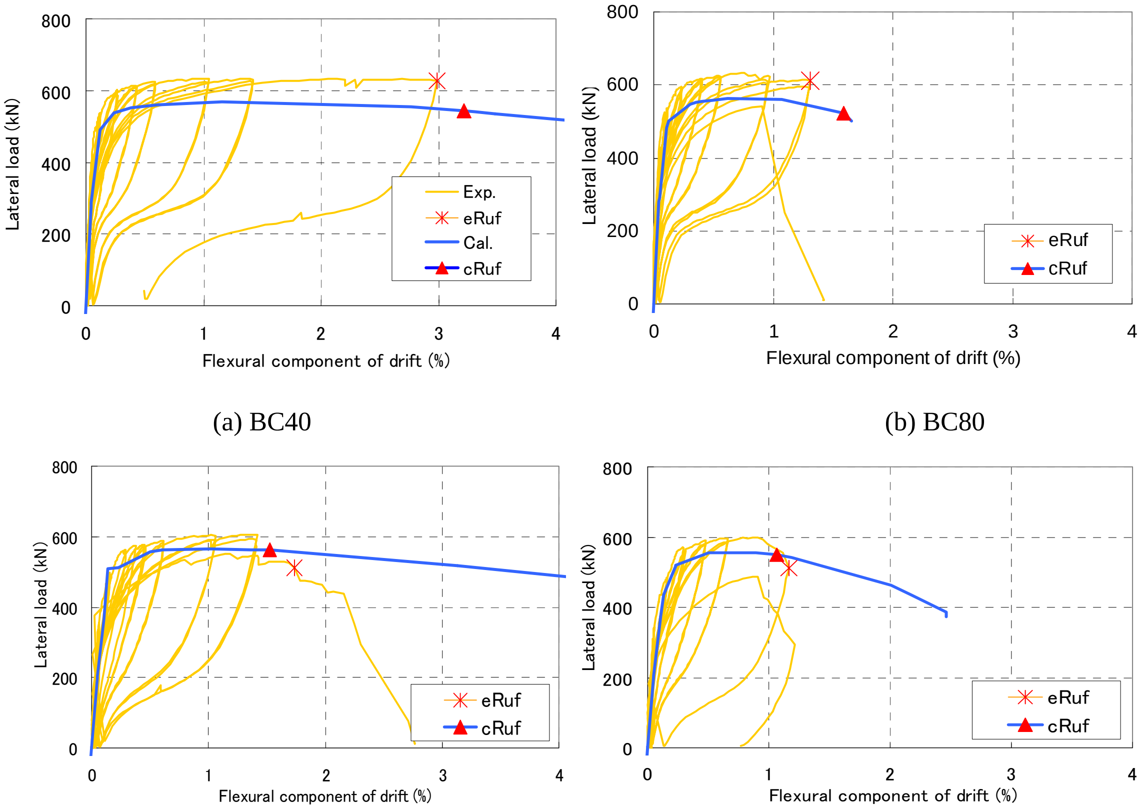

(a) BC40 (b) BC80

(c) NC40 (d) NC80

Figure 7. Simulated lateral load - drift relations compared with experimental results

4. CONCLUSIONS

Four cantilever type structural wall specimens with or without boundary columns were tested with two levels of the end-region shear reinforcement to see their ultimate deformation capability.

- Walls with boundary columns (barbell-shape section) have larger ultimate drift angle while the shear reinforcement ratio of columns was less than that of confined region of rectangular wall. The final failure mode of barbell-shape section walls was more brittle than that of rectangular section walls. Concrete crushing spread widely over the lower portion and buckling of compression zone accompanied for rectangular section walls.
- Flexure deformation is continuously dominant for rectangular section walls while its contribution of flexural drift increased as walls deformed for barbell-shape section walls.
- Simple section analysis combined with plastic hinge length is able to provide relatively accurate backbone curve with the ultimate drift angle.

AKCNOWLEDGEMENT

This research work was financially supported by the Ministry of Land, Infrastructure, Transportation and Tourism.

REFERENCES

Architectural Institute of Japan. (1999). Design Guidelines for Earthquake Resistant Reinforced Concrete Buildings Based on Inelastic Displacement Concept, Chapter 5 Design for flexure and axial force, pp. 119 - 131. (In Japanese)

Mander, J.B., Priestley, M.J.N., and Park, R., (1988). Observed Stress-Strain Behavior of Confined Concrete, Journal of Structural Engineering, ASCE, Vol. 114, No. 8, pp. 1827-1849.

Popovics, S., (1973). A numerical approach to the complete stress-strain curve of concrete, Cement Concrete Research, No. 3, pp. 583-599.

Sakino, K. and Sun, Y., (1994). Stress-strain curve of concrete confined by rectilinear hoop, J. Structural and Construction Engineering, Architectural Institute of Japan, No. 461, pp. 95-104. (In Japanese)